MATERIALS ENGINEERING

10.1126/sciadv.1600067

Quasi-freestanding epitaxial silicene on Ag(111) by oxygen intercalation

Yi Du,[1]* Jincheng Zhuang,[1] Jiaou Wang,[2] Zhi Li,[1] Hongsheng Liu,[3] Jijun Zhao,[3]* Xun Xu,[1] Haifeng Feng,[1] Lan Chen,[4] Kehui Wu,[4] Xiaolin Wang,[1] Shi Xue Dou[1]

Silicene is a monolayer allotrope of silicon atoms arranged in a honeycomb structure with massless Dirac fermion characteristics similar to graphene. It merits development of silicon-based multifunctional nanoelectronic and spintronic devices operated at room temperature because of strong spin-orbit coupling. Nevertheless, until now, silicene could only be epitaxially grown on conductive substrates. The strong silicene-substrate interaction may depress its superior electronic properties. We report a quasi-freestanding silicene layer that has been successfully obtained through oxidization of bilayer silicene on the Ag(111) surface. The oxygen atoms intercalate into the underlayer of silicene, resulting in isolation of the top layer of silicene from the substrate. In consequence, the top layer of silicene exhibits the signature of a 1 × 1 honeycomb lattice and hosts massless Dirac fermions because of much less interaction with the substrate. Furthermore, the oxidized silicon buffer layer is expected to serve as an ideal dielectric layer for electric gating in electronic devices. These findings are relevant for the future design and application of silicene-based nanoelectronic and spintronic devices.

INTRODUCTION

Silicene, in a similar way to graphene, should exhibit exciting and rich physics from theoretical calculations, including massless Dirac fermions, the quantum spin Hall effect, and possible superconductivity (*1*–*10*). In equilibrium low-buckled silicene, silicon atoms adopt sp^2/sp^3-mixed hybridization states (*11*), which require an appropriate substrate to saturate their out-of-plane dangling bonds. This seems to be the reason that monolayer silicene sheets must be fabricated on several conductive substrates by epitaxial growth (*2*–*5*). However, the strong silicene-substrate interaction may markedly depress the superior electronic properties in this two-dimensional (2D) material (*12*, *13*). For example, the hybridization between Ag and Si orbitals results in a surface metallic band and depresses the Dirac fermion characteristics in an epitaxial silicene layer on an Ag(111) surface (*13*). Moreover, the conductive substrates make it difficult to modulate the Fermi level of silicene by electric gating, and this hinders integration of silicene into microelectronic devices. Hence, how to eliminate or minimize substrate effects on the structural and electronic characteristics of epitaxial silicene has become a critical issue for the development of silicene devices. Although some theoretical proposals have been put forward to achieve quasi-freestanding silicene on inert substrates (*14*–*16*), so far, there has barely been any experimental success.

In bilayer silicene on Ag(111), the top $\sqrt{3} \times \sqrt{3}$ layer (with respect to 1 × 1 silicene) is considered to be fabricated on the $\sqrt{13} \times \sqrt{13}/4 \times 4$ layer [with respect to 1 × 1 Ag(111)] (*17*). Therefore, the lower $\sqrt{13} \times \sqrt{13}/4 \times 4$ layer can be regarded as a buffer layer. Convincing experimental evidence suggests that the $\sqrt{3} \times \sqrt{3}$ layer has more sp^2 hybridization states and excellent chemical stability (*18*), whereas the $\sqrt{13} \times \sqrt{13}/4 \times 4$ layer is highly sensitive to ambient gases, especially O_2 (*19*–*21*). Recently, elimination of the graphene-substrate interaction has been achieved by exfoliating epitaxial graphene from an SiC(0001) surface by using hydrogen or fluorine intercalation in the buffer layer (*22*, *23*). Motivated by such a successful strategy, the interaction between the top $\sqrt{3} \times \sqrt{3}$ silicene layer and the metal substrate is expected to be effectively reduced by an appropriate intercalation into the buffer $\sqrt{13} \times \sqrt{13}/4 \times 4$ silicene layer, which, in turn, may allow the top layer to recover the intrinsic properties of silicene.

Here, we conducted oxidization of bilayer silicene on Ag(111) and found that the oxygen molecules intercalate into the $\sqrt{13} \times \sqrt{13}/4 \times 4$ buffer layer of silicene. As a result, the top layer of silicene exhibits the signature of the 1 × 1 lattice structure of "freestanding" silicene and shows a robust Dirac fermion characteristic with less electron doping, which are revealed by scanning tunneling microscopy (STM), x-ray photoemission spectroscopy (XPS), and angle-resolved photoemission spectroscopy (ARPES) measurements. By combining these results with first-principles calculations, we demonstrate that the top layer of silicene can act as quasi-freestanding silicene with weakened interaction with the substrate. Our study establishes a novel and simple way to obtain quasi-freestanding silicene on a substrate. In addition, the silicon oxide buffer layer may be used as the dielectric layer for possible direct construction of field effect transistors (FETs) on the metal substrate.

RESULTS

Figure 1A shows an STM image of pristine $\sqrt{3} \times \sqrt{3}$ silicene supported by the $\sqrt{13} \times \sqrt{13}/4 \times 4$ buffer layer on Ag(111). In the pristine sample, the exposed silicene buffer layer shows three distinct structures, that is, 4 × 4, $\sqrt{13} \times \sqrt{13}R13.9^o$ (–I), and $\sqrt{13} \times \sqrt{13}R19.1^o$ (–II) (*24*). The top layer of silicene exhibits a $\sqrt{3} \times \sqrt{3}$ lattice with a lattice constant a = 0.64 nm, which is approximately $\sqrt{3}$ times that of the 1 × 1 silicene structure (a = 0.38 nm) (*25*). Figure 1B is an STM image of a single piece of silicene island with a top $\sqrt{3} \times \sqrt{3}$ layer, collected after the sample was exposed to oxygen with a dose of 600 Langmuir (L). The bright area of the island is higher than the dark area by about 0.9 Å, as shown in Fig. 1C. The high-resolution STM image (Fig. 1D)

[1]Institute for Superconducting and Electronic Materials, Australian Institute for Innovative Materials, University of Wollongong, Wollongong, New South Wales 2525, Australia. [2]Beijing Synchrotron Radiation Facility, Institute of High Energy Physics, Chinese Academy of Sciences, Beijing 100049, P. R. China. [3]Key Laboratory of Materials Modification by Laser, Ion, and Electron Beams (Dalian University of Technology), Ministry of Education, Dalian 116024, China. [4]Institute of Physics, Chinese Academy of Sciences, Haidian District, Beijing 100080, China.
*Corresponding author. Email: yi_du@uow.edu.au (Y.D.); zhaojj@dlut.edu.cn (J.Z.)

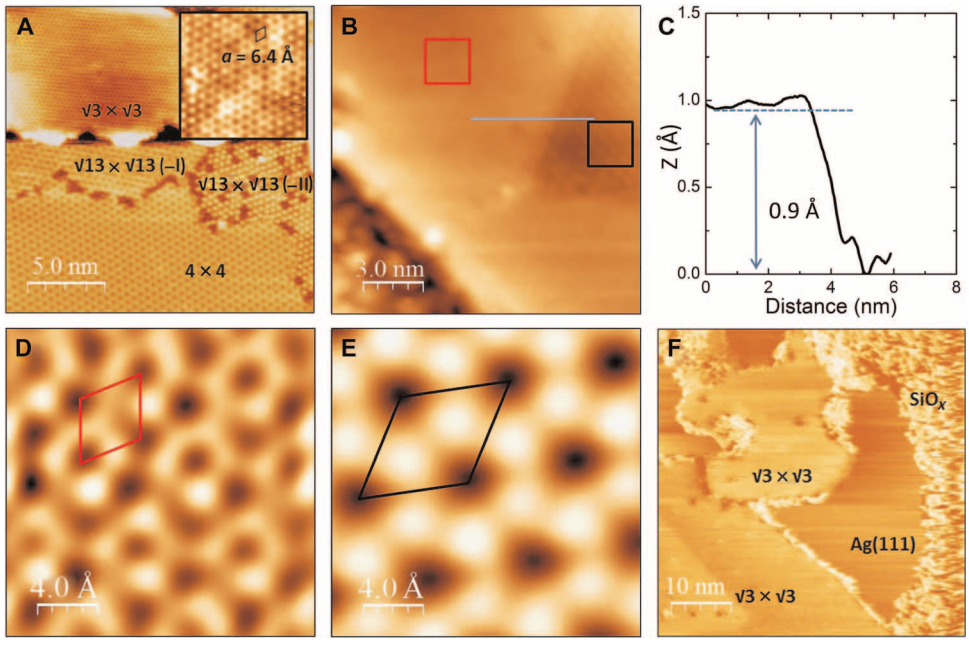

Fig. 1. Topographic images of pristine and oxygen-intercalated epitaxial silicene grown on Ag(111). (**A**) STM topographic image of pristine √3 × √3 silicene that was formed on a √13 × √13/4 × 4 buffer layer. Inset is a high-resolution image of √3 × √3 silicene, which demonstrates a honeycomb structure with a lattice constant of 0.64 nm (V_{bias}= −0.8 V, I = 0.2 nA). (**B**) Oxygen-intercalated √3 × √3 silicene after an oxygen dose of 600 L (V_{bias} = 0.6 V, I = 2 nA). (**C**) Line profile for the straight line in (B). (**D** and **E**) Enlarged STM images of intercalated region [red frame in (B)] and nonintercalated √3 × √3 silicene [black frame in (B)], respectively. The red rhombus and black rhombus stand for the unit cells of 1 × 1 silicene and √3 × √3 silicene, respectively (V_{bias} = 3 mV, I = 4 nA). (**F**) Oxygen-intercalated silicene layers after an oxygen dose of 1200 L, in which the buffer layer is fully oxidized, whereas the √3 × √3 silicene shows robust structural stability against oxygen intercalation (V_{bias} = −1.2 V, I = 0.1 nA).

reveals that the structural features of the √3 × √3 reconstruction in the higher area are weaker than those in the dark area (Fig. 1E). It is found that the higher area forms from the edge of a √3 × √3 silicene flake. The higher area exhibits the signature of a 1 × 1 lattice of freestanding silicene. To the best of our knowledge, this is the first experimental observation of a 1 × 1 lattice in silicene. We further increased the oxygen dose up to 1200 L, and the corresponding STM image (Fig. 1F) shows that the exposed √13 × √13/4 × 4 layer changes to an amorphous form, whereas the √3 × √3 silicene clearly remains intact. The higher degree of buckling of Si atoms in the √13 × √13/4 × 4 silicene layer (*19*) enables surface dangling bonds to easily react with oxygen. Consequently, crumpled amorphous silicon oxide (SiO_x) is formed, leading to exposure of the bare Ag(111) surface, which was also observed in our previous study (*19*). Considering the top √3 × √3 layer sitting on the √13 × √13/4 × 4 layer, we conjecture that the oxygen atoms are intercalated between the two silicene layers and react with the underlying √13 × √13/4 × 4 layer. That is why the surface of the top √3 × √3 layer remains intact and the oxidized area of the √3 × √3 layer is higher than the unoxidized area. The increased height reflects the fact that the oxidizing process of the √13 × √13/4 × 4 layer follows the conventional oxidation of silicon, in which the volume of SiO_x is increased upon oxidation. It should be noted that all the silicon atoms in √3 × √3 silicene form a honeycomb pattern in the high-resolution STM image, that is, the 1 × 1 lattice of freestanding silicene, as schematically illustrated in fig. S1, whereas the arrangement of top silicon atoms still reflects the √3 × √3 superstructure, indicating that the √3 × √3 superstructure is derived from 1 × 1 silicene. Thus, the observation of a 1 × 1 lattice of freestanding silicene in the oxidized area of the √3 × √3 layer suggests that the interactions between the top layer of silicene and the underlying silicene/silicon oxide or Ag(111) substrate are weakened by oxidization.

To corroborate the oxidization model sketched in Fig. 1, a detailed analysis of the chemical bonds was conducted by XPS and Raman spectroscopy. Si 2*p* and Ag 3*d* core-level spectra were collected for the pristine and oxygen-treated silicene samples, as shown in Fig. 2A and fig. S2. Different components contributing to the spectra were decomposed by a curve-fitting procedure (*13*). We determined the signature of XPS peak positions corresponding to the √13 × √13/4 × 4 buffer layer in our previous work (*13*). Therefore, we categorize the two kinds of bonding components into groups, that is, group I (√3 × √3 silicene, labeled as Si_1 and Si_2) and group II (√13 × √13/4 × 4 silicene buffer layer, labeled as Si_3 and Si_4) from the fitting of the Si 2*p* lines. We emphasize the decreased intensities and obvious shifts of the group II components after oxygen treatment, whereas the group I components do not show any variation. This indicates that the Si–Ag bonds between the √13 × √13/4 × 4 buffer layer and the Ag(111) surface are partially broken by oxygen treatment, whereas the top √3 × √3 silicene layer resists oxidization. The broad SiO_x peak at 101.6 eV accompanies the shift of group II component, verifying that the breaking of the Si–Ag bonds is due to oxidization of the buffer layer (*13*).

Raman spectroscopy is particularly sensitive to changes in the band gap, the in-plane bonds, and the strain effect associated with structural change and, thus, plays an important role in the structural characterization of 2D materials (*26*–*28*). We have identified fingerprint Raman peaks for each silicene phase (*28*). The phonon modes in the pristine and oxygen-intercalated samples were characterized by in situ Raman spectroscopy, as shown in Fig. 2B. Because the Ag(111) substrate is a

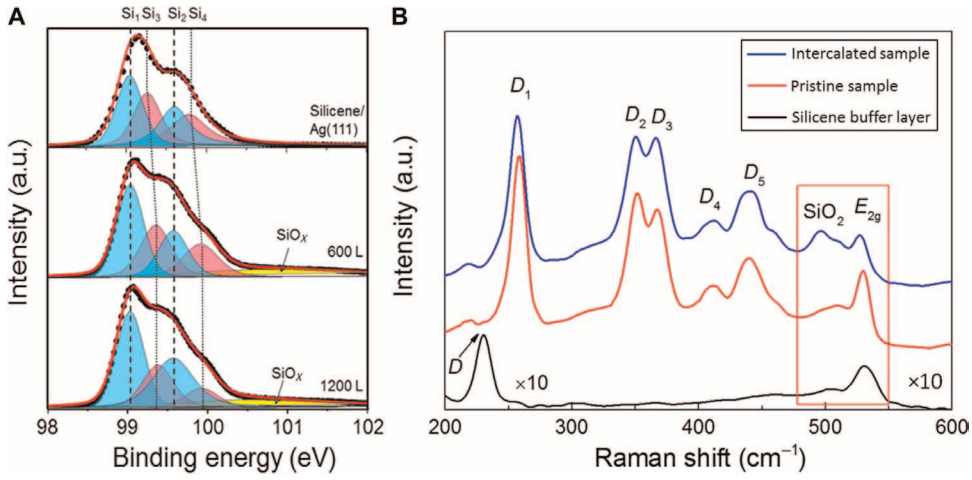

Fig. 2. XPS and Raman spectra of pristine and oxygen-intercalated silicene. (**A**) Si 2*p* core-level XPS spectra of pristine (top) and oxygen-intercalated (middle, lower dose; bottom, higher dose) silicene layers grown on Ag(111). The Si_1 and Si_2 peaks are attributed to Si–Si bonds in $\sqrt{3} \times \sqrt{3}$ silicene, whereas Si_3 and Si_4 are attributed to the $\sqrt{13} \times \sqrt{13}/4 \times 4$ silicene buffer layer. a.u., arbitrary units. (**B**) Raman spectra of $\sqrt{13} \times \sqrt{13}/4 \times 4$ silicene buffer layer (black), $\sqrt{3} \times \sqrt{3}$ silicene with 0.3 monolayer coverage on $\sqrt{13} \times \sqrt{13}/4 \times 4$ buffer layer (pristine sample; red), and oxygen-intercalated sample (blue). The oxidized buffer layer features a broad Raman peak at 494 cm^{-1} in the spectrum of the oxygen-intercalated sample.

metal, which does not contribute a Raman signal, the Raman spectra are only attributed to the epitaxial silicene layers, although the thicknesses of the silicene layers are thinner than the penetration depth of Raman incident light. The Raman peak at 526.3 ± 3 cm^{-1} is due to the doubly degenerate E_{2g} mode (*27*, *28*) at the Brillouin zone (BZ) center Γ point for all silicene structures. The E_{2g} peak of silicene, regardless of structure, is sensitive to the temperature variation. The in situ temperature-dependent Raman spectra of a monolayer $4 \times 4/\sqrt{13} \times \sqrt{13}$ buffer layer and a $\sqrt{3} \times \sqrt{3}$ silicene sample from liquid nitrogen temperature to 275 K are shown in fig. S3. It is found that the E_{2g} mode in both samples shows an obvious blue shift when the temperature is decreased, which is possibly attributable to the thermal expansion effect. In contrast to the $\sqrt{13} \times \sqrt{13}/4 \times 4$ structure, the $\sqrt{3} \times \sqrt{3}$ silicene exhibits a more sensitive E_{2g} mode under temperature variation from 80 to 275 K. The D_1-D_5 peaks are attributed to electron inter- or intravalley scattering at the zigzag and armchair edges in the $\sqrt{3} \times \sqrt{3}$ silicene, and the D peak is induced by boundary defects in the $\sqrt{13} \times \sqrt{13}/4 \times 4$ silicene (*28*). After oxygen treatment, the D peak vanishes, and an additional Raman peak at 494 cm^{-1} emerges, which indicates the formation of amorphous silicon oxide (*29*). In contrast, all the Raman peaks assigned to the $\sqrt{3} \times \sqrt{3}$ silicene are almost invariable after oxygen treatment. By scrutinizing the fingerprint E_{2g} peak, it is found that the peak position is blue-shifted by 4 cm^{-1} in the oxygen-intercalated sample. The shift of the Raman signal suggests that the tensile strain in epitaxial $\sqrt{3} \times \sqrt{3}$ silicene is "released" toward "unstrained" freestanding 1×1 silicene by oxygen intercalation (*27*, *28*, *30*). Ex situ Raman spectra were used to examine the stability of the oxygen-intercalated sample exposed to ambient air. The detailed results are displayed in fig. S4, in which we demonstrate that the intercalated $\sqrt{3} \times \sqrt{3}$ silicene survives in the ambient environment for at least 120 hours.

DISCUSSION

The STM, XPS, and Raman spectroscopy results suggest that the oxygen atoms are intercalated between the silicene layers and weaken the interaction between the top layer and the Ag(111) surface. This picture is confirmed by our density functional theory (DFT) calculations on the oxidation of silicene layers on the Ag(111) surface. As shown in Fig. 3A, when an O_2 molecule is adsorbed on monolayer 4×4 silicene/Ag(111), it would spontaneously decompose into two O atoms, with one O atom sitting on the top of a silicon atom and the other located at the neighboring bridge site. The chemical dissociation of a gaseous O_2 molecule on monolayer 4×4 silicene is an exothermic process with adsorption energy of 5.474 eV. In sharp contrast, when an O_2 molecule is adsorbed on the $\sqrt{3} \times \sqrt{3}$ silicene layer on top of 4×4 silicene/Ag(111), it would not decompose after relaxation, as shown in Fig. 3B. The corresponding adsorption energy of only 2.84 eV is much smaller than that for the dissociative adsorption of O_2 on the monolayer 4×4 silicene (5.474 eV), indicating the higher resistance of $\sqrt{3} \times \sqrt{3}$ silicene to oxidation compared with monolayer 4×4 silicene, as observed in our experimental results.

It is necessary to determine the status of the buffer layer beneath $\sqrt{3} \times \sqrt{3}$ silicene before simulating the interaction strength after oxygen intercalation. We directly placed an O_2 molecule between the top $\sqrt{3} \times \sqrt{3}$ layer and the bottom 4×4 layer in bilayer silicene (Fig. 3C). Upon relaxation, O_2 would spontaneously dissociate into two oxygen atoms, and the adsorption energy is as large as 6.36 eV, comparable to the adsorption energy of the uncovered buffer layer. The even larger adsorption energy for the covered buffer layer suggests the preference for oxidization of the covered $\sqrt{13} \times \sqrt{13}/4 \times 4$ silicene layer underneath the top $\sqrt{3} \times \sqrt{3}$ silicene layer, as shown in the schematic diagrams in fig. S5B. The dynamic process of oxygen intercalation is further experimentally revealed in fig. S6, where the intercalation depth, which is the distance from the silicene edges to the centers of the top $\sqrt{3} \times \sqrt{3}$ silicene islands, increases with increasing oxygen dose.

To model the oxidized bilayer silicene on Ag(111) substrate, we constructed a sandwich structure of $\sqrt{3} \times \sqrt{3}$ silicene/SiO_x/Ag(111) ($x = 1.909$), as depicted in Fig. 3D. After relaxation, the top silicene sheet retains its hexagonal honeycomb lattice (Fig. 3E) and interacts weakly with the SiO_x buffer layer at an average separation of 3.09 Å. Compared to the interfacial binding energy (123 meV/$Å^2$) between the top and the bottom

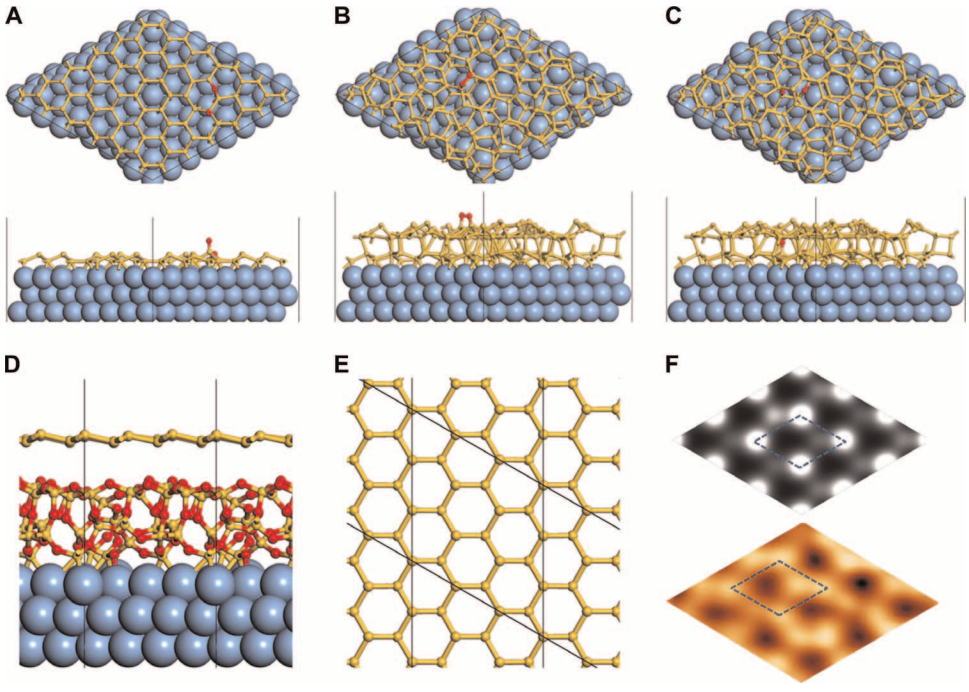

Fig. 3. Simulations for atomic structures of oxygen adsorbed on both buffer layer and top layer silicene. (**A** to **C**) Atomic structures of an O_2 molecule adsorbed on 4 × 4 silicene buffer layer (A), top layer silicene (B), and 4 × 4 buffer layer underneath √3 × √3 silicene (C). (**D** and **E**) Atomic structure of silicene/SiO_x/Ag(111) from ab initio molecular dynamics (AIMD) simulation: side view (D) and top view (E) of the top layer silicene only. (**F**) Simulated (top) and experimental (bottom) high-resolution STM images of silicene/SiO_x/Ag(111), showing the 1 × 1 silicene honeycomb lattice.

layer of the pristine bilayer silicene, the binding energy (12 meV/Å^2) between the silicene top layer and the SiO_x buffer layer is significantly reduced by one order of magnitude after oxygen intercalation. As a consequence of the weakened silicene-substrate interaction, the simulated STM image (Fig. 3F), based on the structural model of silicene/SiO_x/Ag(111) in Fig. 3D, coincides with the experimental one, showing the clear pattern of the 1 × 1 structure of the honeycomb lattice of silicene. Therefore, DFT calculations convincingly support the existence of a quasi-freestanding silicene top layer after oxygen intercalation, as conjectured from our experiments.

Apart from the structural aspect, oxygen intercalation has a remarkable impact on the electronic structure of silicene layers. Figure 4 shows the electronic band structures measured by ARPES on pristine silicene and oxygen-intercalated silicene grown on Ag(111). As a reference, the electronic band structure of the clean Ag(111) surface is also shown in Fig. 4A, where the Shockley surface state (SSS) at the BZ center (Γ point) and the bulk Ag *sp* band are indicated. When √3 × √3 silicene was grown, we observed two faint bands with linear dispersion crossing at the Γ point, as shown in Fig. 4B. Constant energy cuts of the spectral function at different binding energies confirm that both bands originate from a Dirac cone structure, as shown in Fig. 4E, which can be assigned to the linear π and π* states of √3 × √3 silicene (*17*, *31*). The Dirac point (DP) is located at about 0.33 eV below the Fermi level (E_F) due to electron doping from the Ag(111) substrate (*32*).

Figure 4 (C and D) presents the electronic band structures after oxygen intercalation under different doses of oxygen (600 and 1200 L) at 200°C, as measured by ARPES with higher energy and momentum resolutions. One can clearly see that two single Dirac cones meet at the DP, which is located at about −0.28 and −0.26 eV for the samples exposed to oxygen doses of 600 and 1200 L, respectively. The characteristic "Δ"-shaped bands at a deep energy level (below −0.7 eV), which were attributed to the hybridization between interface Si p_z orbitals and Ag *d* orbitals in the pristine sample (*12*, *13*), are smeared or vanish after oxygen intercalation, although the typical bulk *sp* band of Ag across the Fermi level at k = 1.15 Å^{-1} appeared in the ARPES results after oxygen intercalation. The ARPES results in figs. S7 and S8 indicate that this band remains stable under oxygen intercalation. A new state corresponding to silicon oxide appears in the oxygen-intercalated silicene at a deep energy level (below −0.6 eV), centered at k = −0.2 Å along the Γ-K direction. This state is more obvious in the ARPES feature for the oxygen-intercalated sample after an oxygen dose of 1200 L, as shown in Fig. 4D.

The ARPES results reveal that the electronic structures of epitaxial silicene are modulated by chemical adsorption. In the initial intercalation stage, the chemical interaction between the buffer layer silicene and the Ag substrate is broken by the oxygen atoms. The Si–Ag hybridized state in the silicene/Ag(111) system is replaced by electronic states attributable to Si–O bonds. As the oxygen dose increases, the oxidized √13 × √13/4 × 4 buffer layer contributes more states in the deep level (below −0.6 eV). Meanwhile, the DP is pushed up toward the Fermi level, because the oxidized buffer layer acts as a dielectric barrier and lowers the electron doping in the top √3 × √3 silicene layer, as shown in Fig. 4F. The thickness of the oxidized buffer layer is increased when the oxygen dose is increased. That is, the dielectric barrier will become thicker with increasing oxygen dose. Consequently, the doping level should be lower in the intercalated silicene with a higher oxygen dose. This agrees with our ARPES results, in which 1200-L oxygen–intercalated silicene has its DP at 0.26 eV below the Fermi level, whereas 600-L oxygen–intercalated silicene shows its DP at 0.28 eV below the Fermi level. The weakened doping effect from the substrate on the silicene's electronic structure

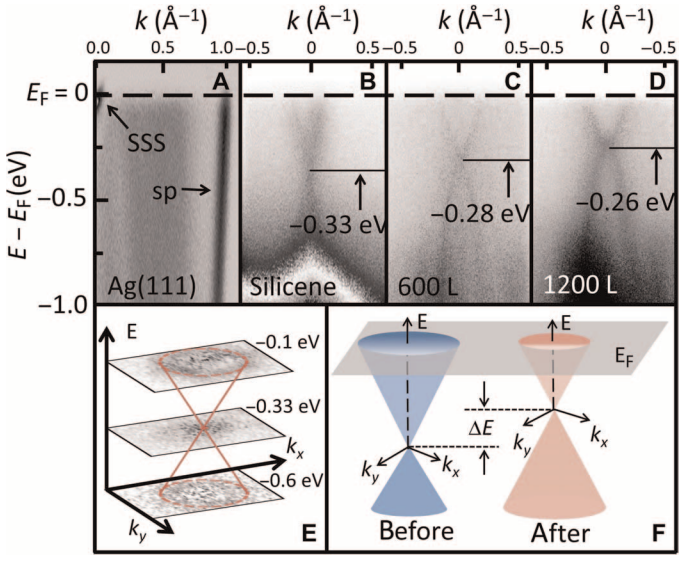

Fig. 4. ARPES results of pristine and oxygen-intercalated silicene. (**A** to **D**) Energy versus *k* dispersion measured by ARPES for clean Ag(111) surface (A), as-grown $\sqrt{3} \times \sqrt{3}$ silicene formed on buffer layer (B), oxygen-intercalated silicene with an oxygen dose of 600 L (C), and intercalated silicene with an oxygen dose of 1200 L (D). The SSS and the *sp* band in (A) are attributed to the Ag(111) substrate. The DP in (B) to (D) is lifted up with increased oxygen dose from 0 to 1200 L, indicating less electron doping from the Ag(111) substrate due to oxygen intercalation. (**E**) ARPES energy cuts reveal a Dirac cone structure in pristine silicene. (**F**) Schematic view of shifting of Dirac cone due to oxygen intercalation in ARPES measurement.

is also observed in the scanning tunneling spectroscopy (STS) results (fig. S9).

On the basis of the ARPES results, the Fermi velocity is estimated to be about $(4.4 \pm 0.2) \times 10^5$ m/s for the pristine sample, although it decreases to about $(3.9 \pm 0.5) \times 10^5$ m/s and $(3.4 \pm 0.5) \times 10^5$ m/s for the 600-L and 1200-L oxygen–intercalated silicene, respectively. In the intercalated silicene, the tensile strain is released, which increases the degree of buckling and weakens sp^2 hybridization of Si atoms (*33*), thus decreasing the hopping parameter *t* within a two-band tight-binding picture (*34*). As a consequence, the Fermi velocity $v_F = 3ta/2$ is expectedly lower in freestanding silicene (with small *a* and *t*) than in epitaxial silicene. The observed decreases in Fermi velocity are most likely attributed to the oxygen intercalation process. The ARPES measurements indicate that the $\sqrt{3} \times \sqrt{3}$ silicene layer has a high resistance to oxidation and that its Dirac cone structure is robust during oxygen intercalation. The DFT band structure calculations based on the structural model of silicene/SiO_x/Ag (Fig. 3D) also show the existence of the characteristic Dirac cone of quasi-freestanding silicene around the Fermi level, with a mini-gap of 20 meV opened at the Dirac cone because of weak interaction between the top silicene layer and the SiO_x buffer layer (fig. S10). Analysis of the partial density of state further indicates that the top silicene layer exhibits semimetal characteristics like freestanding silicene, and the SiO_x buffer layer is insulating with about a 5-eV gap (fig. S11). Finally, our results suggest that the insulating SiO_x buffer layer provides a barrier for electric gating that can be directly used in FETs. This is significant for the integration of silicene in future microelectronic devices.

In summary, we have demonstrated an effective method to make epitaxial silicene quasi-freestanding from its Ag(111) substrate by oxygen intercalation. The highly reactive $\sqrt{13} \times \sqrt{13}$ and 4×4 silicene interfacial layers can be fully oxidized, resulting in decoupling of the top silicon atoms from the Ag substrate. Meanwhile, the top $\sqrt{3} \times \sqrt{3}$ silicene layer shows chemical resistance to oxygen, which ensures retention of the honeycomb structure and the characteristic massless Dirac fermions after oxygen intercalation. The intercalation opens up the possibility of producing quasi-freestanding and transferrable epitaxial silicene. Moreover, the oxidized $\sqrt{13} \times \sqrt{13}/4 \times 4$ silicene buffer layer (SiO_x) holds promise for peeling off and transferring epitaxial silicene to another dielectric support to make electronic devices.

MATERIALS AND METHODS

Sample preparation

The silicene layers were fabricated by the deposition of silicon atoms on Ag(111) substrate from a heated silicon wafer in a preparation chamber attached to an in situ STM/Raman system under ultrahigh vacuum (UHV; $<1 \times 10^{-10}$ torr). A clean Ag(111) substrate was prepared by argon ion sputtering and subsequently annealed at 550°C for several cycles. The deposition flux of Si was 0.08 monolayer per minute. The temperature of the Ag(111) substrate was kept at 220°C during deposition (*19*, *35*). An in situ oxygen intercalation process was carried out by introducing oxygen molecules into the preparation chamber at a sample temperature of 200°C. Langmuir was used as the unit of exposure to O_2, that is, 1 L was an exposure of O_2 (10^{-6} torr) in 1 s.

Characterization of structural and electronic properties

The STM and Raman spectroscopy measurements were carried out using a low-temperature UHV STM/scanning near-field optical microscopy system (SNOM1400, Unisoku Co.) in UHV ($<8 \times 10^{-11}$ torr) at 77 K. The Raman spectra were acquired using a laser excitation of 532 nm (2.33 eV) delivered through a single-mode optical fiber at 77 K in UHV. The spot size of the incident laser in the in situ Raman spectroscopy was about 3 μm in diameter. In situ ARPES and XPS characterizations were performed at the Photoelectron Spectroscopy Station in the Beijing

Synchrotron Radiation Facility (BSRF) using a SCIENTA R4000 analyzer. A monochromatized He I light source (21.2 eV) was used for the band dispersion measurements. The total energy resolution was set to 15 meV, and the angular resolution was set to ~0.3°, which gives a momentum resolution of ~0.01 π/a. The XPS experiments were performed at Beamline 4B9B, and variable photon energies were referenced to a fresh Au polycrystalline film. The spot size of incident light in XPS was about 1 mm in diameter.

DFT calculations

Ab initio calculations were performed using DFT and a plane-wave basis with a cutoff energy of 400 eV, as implemented in Vienna Ab initio Simulation Package (*36*). The electron-ion interactions were represented by projector augmented wave potentials (*37*). The Perdew-Burke-Ernzerhof functional was adopted to describe the exchange-correlation interactions (*38*). To properly take into account the long-range van der Waals interactions in layered structures, the DFT-D3 scheme (*39*) was used. The Ag(111) surface was modeled by a three-layer slab model with a vacuum space of more than 12 Å, which was cleaved from a face-centered cubic solid silver bulk with an experimental lattice constant of 2.89 Å. Within the constrained supercell, the slab model was further relaxed, with the bottom layer fixed to mimic a semi-infinite solid. The monolayer 4 × 4 silicene/Ag(111) superstructure was composed of 3 × 3 silicene cells and 4 × 4 Ag(111) cells. Bilayer silicene was further constructed by putting a $\sqrt{3} \times \sqrt{3}$ silicene layer on top of the 4 × 4 silicene/Ag(111). To simulate oxygen adsorption on pristine bilayer silicene, a 2 × 2 supercell of the $\sqrt{3} \times \sqrt{3}$ silicene/4 × 4 silicene/Ag(111) structure with lattice constant of 23.12 Å and a total of 192 silver atoms plus 150 silicon atoms was adopted. Similarly, a 2 × 2 supercell of monolayer 4 × 4 silicene on Ag(111) was also considered. To model oxygen intercalation, a slab of 4 × 4 Ag(111) supercell with 48 silver atoms, a buffer layer of SiO_x with 22 silicon atoms and 42 oxygen atoms, and a top 1 × 1 silicene layer with 18 silicon atoms were combined to construct the silicene/SiO_x/Ag(111) hybrid structure, which was relaxed by an AIMD simulation at 550 K for 10 ps followed by geometry optimization. Note that the SiO_x buffer layer was thicker than the pristine 4 × 4 silicene layer, based on our experimental observation that the height of an oxygen-intercalated silicene area was higher than that of the pristine silicene area (see the Supplementary Materials).

SUPPLEMENTARY MATERIALS

Supplementary material for this article is available at http://advances.sciencemag.org/cgi/content/full/2/7/e1600067/DC1

fig. S1. Observation of 1 × 1 lattice induced by oxygen intercalation.
fig. S2. XPS spectra of oxygen-intercalated silicene.
fig. S3. In situ temperature-dependent Raman spectra of silicene samples in different structures.
fig. S4. Ex situ Raman spectra of oxygen-intercalated samples exposed to ambient air.
fig. S5. STM results on intercalated silicene layers.
fig. S6. STM images of samples after oxygen intercalation under different doses and STS *dI*/*dV* measurements.
fig. S7. Additional ARPES results on intercalated silicene under an oxygen dose of 600 L.
fig. S8. ARPES results on silicene buffer layer grown on Ag(111).
fig. S9. STS in intercalated and pristine areas of silicene.
fig. S10. DFT results on the electronic band structure of oxygen-intercalated bilayer silicene.
fig. S11. DFT results on the partial density of states of bilayer silicene before and after oxygen intercalation.

REFERENCES AND NOTES

1. S. Cahangirov, M. Topsakal, E. Aktürk, H. Şahin, S. Ciraci, Two- and one-dimensional honeycomb structures of silicon and germanium. *Phys. Rev. Lett.* **102**, 236804 (2009).
2. P. Vogt, P. De Padova, C. Quaresima, J. Avila, E. Frantzeskakis, M. C. Asensio, A. Resta, B. Ealet, G. Le Lay, Silicene: Compelling experimental evidence for graphenelike two-dimensional silicon. *Phys. Rev. Lett.* **108**, 155501 (2012).
3. B. Feng, Z. Ding, S. Meng, Y. Yao, X. He, P. Cheng, L. Chen, K. Wu, Evidence of silicene in honeycomb structures of silicon on Ag(111). *Nano Lett.* **12**, 3507–3511 (2012).
4. A. Fleurence, R. Friedlein, T. Ozaki, H. Kawai, Y. Wang, Y. Yamada-Takamura, Experimental evidence for epitaxial silicene on diboride thin films. *Phys. Rev. Lett.* **108**, 245501 (2012).
5. L. Meng, Y. Wang, L. Zhang, S. Du, R. Wu, L. Li, Y. Zhang, G. Li, H. Zhou, W. A. Hofer, H.-J. Gao, Buckled silicene formation on Ir(111). *Nano Lett.* **13**, 685–690 (2013).
6. G. G. Guzmán-Verri, L. C. Lew Yan Voon, Electronic structure of silicon-based nanostructures. *Phys. Rev. B* **76**, 075131 (2007).
7. L. Tao, E. Cinquanta, D. Chiappe, C. Grazianetti, M. Fanciulli, M. Dubey, A. Molle, D. Akinwande, Silicene field-effect transistors operating at room temperature. *Nat. Nanotechnol.* **10**, 227–231 (2015).
8. H. Pan, Z. Li, C.-C. Liu, G. Zhu, Z. Qiao, Y. Yao, Valley-polarized quantum anomalous Hall effect in silicene. *Phys. Rev. Lett.* **112**, 106802 (2014).
9. F. Liu, C.-C. Liu, K. Wu, F. Yang, Y. Yao, *d+id'* chiral superconductivity in bilayer silicene. *Phys. Rev. Lett.* **111**, 066804 (2013).
10. L. Chen, B. Feng, K. Wu, Observation of a possible superconducting gap in silicene on Ag(111) surface. *Appl. Phys. Lett.* **102**, 081602 (2013).
11. E. Cinquanta, E. Scalise, D. Chiappe, C. Grazianetti, B. van den Broek, M. Houssa, M. Fanciulli, A. Molle, Getting through the nature of silicene: An sp^2–sp^3 two-dimensional silicon nanosheet. *J. Phys. Chem. C* **117**, 16719–16724 (2013).
12. D. Tsoutsou, E. Xenogiannopoulou, E. Golias, P. Tsipas, A. Dimoulas, Evidence for hybrid surface metallic band in (4 × 4) silicene on Ag(111). *Appl. Phys. Lett.* **103**, 231604 (2013).
13. X. Xu, J. Zhuang, Y. Du, H. Feng, N. Zhang, C. Liu, T. Lei, J. Wang, M. Spencer, T. Morishita, X. Wang, S. X. Dou, Effects of oxygen adsorption on the surface state of epitaxial silicene on Ag(111). *Sci. Rep.* **4**, 7543 (2014).
14. H. Liu, J. Gao, J. Zhao, Silicene on substrates: A way to preserve or tune its electronic properties. *J. Phys. Chem. C* **117**, 10353–10359 (2013).
15. S. Kokott, P. Pflugradt, L. Matthes, F. Bechstedt, Nonmetallic substrates for growth of silicene: An ab initio prediction. *J. Phys. Condens. Matter* **26**, 185002 (2014).
16. J. Zhu, U. Schwingenschlögl, Structural and electronic properties of silicene on MgX_2 (X = Cl, Br, and I). *ACS Appl. Mater. Interfaces* **6**, 11675–11681 (2014).
17. P. De Padova, P. Vogt, A. Resta, J. Avila, I. Razado-Colambo, C. Quaresima, C. Ottaviani, B. Olivieri, T. Bruhn, T. Hirahara, T. Shirai, S. Hasegawa, M. C. Asensio, G. Le Lay, Evidence of Dirac fermions in multilayer silicene. *Appl. Phys. Lett.* **102**, 163106 (2013).
18. P. De Padova, C. Ottaviani, C. Quaresima, B. Olivieri, P. Imperatori, E. Salomon, T. Angot, L. Quagliano, C. Romano, A. Vona, M. Muniz-Miranda, A. Generosi, B. Paci, G. Le Lay, 24 H stability of thick multilayer silicene in air. *2D Materials* **1**, 021003 (2014).
19. Y. Du, J. Zhuang, H. Liu, X. Xu, S. Eilers, K. Wu, P. Cheng, J. Zhao, X. Pi, K. W. See, G. Peleckis, X. Wang, S. X. Dou, Tuning the band gap in silicene by oxidation. *ACS Nano* **8**, 10019–10025 (2014).
20. J. Qiu, H. Fu, Y. Xu, A. I. Oreshkin, T. Shao, H. Li, S. Meng, L. Chen, K. Wu, Ordered and reversible hydrogenation of silicene. *Phys. Rev. Lett.* **114**, 126101 (2015).
21. J. Gao, J. Zhao, Initial geometries, interaction mechanism and high stability of silicene on Ag(111) surface. *Sci. Rep.* **2**, 861 (2012).
22. C. Riedl, C. Coletti, T. Iwasaki, A. A. Zakharov, U. Starke, Quasi-free-standing epitaxial graphene on SiC obtained by hydrogen intercalation. *Phys. Rev. Lett.* **103**, 246804 (2009).
23. S. L. Wong, H. Huang, Y. Wang, L. Cao, D. Qi, I. Santoso, W. Chen, A. T. S. Wee, Quasi-free-standing epitaxial graphene on SiC (0001) by fluorine intercalation from a molecular source. *ACS Nano* **5**, 7662–7668 (2011).
24. H. Enriquez, S. Vizzini, A. Kara, B. Lalmi, H. Oughaddou, Silicene structures on silver surfaces. *J. Phys. Condens. Matter* **24**, 314211 (2012).
25. L. Chen, H. Li, B. Feng, Z. Ding, J. Qiu, P. Cheng, K. Wu, S. Meng, Spontaneous symmetry breaking and dynamic phase transition in monolayer silicene. *Phys. Rev. Lett.* **110**, 085504 (2013).
26. Z. Ni, Q. Liu, K. Tang, J. Zheng, J. Zhou, R. Qin, Z. Gao, D. Yu, J. Lu, Tunable bandgap in silicene and germanene. *Nano Lett.* **12**, 113–118 (2012).
27. J.-A. Yan, R. Stein, D. M. Schaefer, X.-Q. Wang, M. Y. Chou, Electron-phonon coupling in two-dimensional silicene and germanene. *Phys. Rev. B* **88**, 121403(R) (2013).
28. J. Zhuang, X. Xu, Y. Du, K. Wu, L. Chen, W. Hao, J. Wang, W. K. Yeoh, X. Wang, S. X. Dou, Investigation of electron-phonon coupling in epitaxial silicene by in situ Raman spectroscopy. *Phys. Rev. B* **91**, 161409(R) (2015).
29. F. L. Galeener, A. E. Geissberger, Vibrational dynamics in ^{30}Si-substituted vitreous SiO_2. *Phys. Rev. B* **27**, 6199–6204 (1983).
30. A. O'Hare, F. V. Kusmartsev, K. I. Kugel, A stable "flat" form of two-dimensional crystals: Could graphene, silicene, germanene be minigap semiconductors? *Nano Lett.* **12**, 1045–1052 (2012).
31. L. Chen, C.-C. Liu, B. Feng, X. He, P. Cheng, Z. Ding, S. Meng, Y. Yao, K. Wu, Evidence for Dirac fermions in a honeycomb lattice based on silicon. *Phys. Rev. Lett.* **109**, 056804 (2012).

32. B. Feng, H. Li, C.-C. Liu, T.-N. Shao, P. Cheng, Y. Yao, S. Meng, L. Chen, K. Wu, Observation of Dirac cone warping and chirality effects in silicene. *ACS Nano* **7**, 9049–9054 (2013).
33. J.-A. Yan, S.-P. Gao, R. Stein, G. Coard, Tuning the electronic structure of silicene and germanene by biaxial strain and electric field. *Phys. Rev. B* **91**, 245403 (2015).
34. A. H. Castro Neto, F. Guinea, N. M. R. Peres, K. S. Novoselov, A. K. Geim, The electronic properties of graphene. *Rev. Mod. Phys.* **81**, 109–162 (2009).
35. Y. Feng, B.-J. Feng, Z.-J. Xie, W.-B. Li, X. Liu, D.-F. Liu, L. Zhao, L. Chen, X.-J. Zhou, K.-H. Wu, Observation of a flat band in silicene. *Chinese Phys. Lett.* **31**, 127303 (2014).
36. G. Kresse, J. Furthmüller, Efficient iterative schemes for ab initio total-energy calculations using a plane-wave basis set. *Phys. Rev. B* **54**, 11169–11186 (1996).
37. G. Kresse, D. Joubert, From ultrasoft pseudopotentials to the projector augmented-wave method. *Phys. Rev. B* **59**, 1758–1775 (1999).
38. J. P. Perdew, K. Burke, M. Ernzerhof, Generalized gradient approximation made simple. *Phys. Rev. Lett.* **77**, 3865–3868 (1996).
39. S. Grimme, J. Antony, S. Ehrlich, H. Krieg, A consistent and accurate ab initio parametrization of density functional dispersion correction (DFT-D) for the 94 elements H-Pu. *J. Chem. Phys.* **132**, 154104 (2010).

Acknowledgments: We acknowledge H. J. Qian and T. Lei at the BSRF for valuable discussions. We thank T. Silver for her valuable comments on this work. **Funding:** This work was supported by the Australian Research Council through Discovery Project grant DP140102581 and Linkage Infrastructure, Equipment and Facilities grants LE100100081 and LE110100099. We would like to acknowledge support by the University of Wollongong through a University Research Council Small Grant in 2014. The work carried out in China was supported by Chinese Academy of Sciences project 1G2009312311750101, the Fundamental Research Funds for the Central Universities of China grant DUT16LAB01, and National Natural Science Foundation of China grants 11134005, 11375228, 11574040, and 11575227. **Author contributions:** Y.D., J.Z., and Z.L. did the sample preparation and STM characterizations. J.W., Y.D., and X.X. did the ARPES and XPS measurements. J.Z. and H.F. did the Raman characterizations. H.L. and J.Z. performed the DFT calculations. L.C., K.W., X.W., and S.X.D. helped with data analysis. Y.D., L.C., and J.Z. designed the experiment plan and wrote the paper. **Competing interests:** The authors declare that they have no competing interests. **Data and materials availability:** All data needed to evaluate the conclusions in the paper are present in the paper and/or the Supplementary Materials. Additional data related to this paper may be requested from the authors.

Submitted 14 January 2016
Accepted 23 June 2016
Published 22 July 2016
10.1126/sciadv.1600067

Citation: Y. Du, J. Zhuang, J. Wang, Z. Li, H. Liu, J. Zhao, X. Xu, H. Feng, L. Chen, K. Wu, X. Wang, S. X. Dou, Quasi-freestanding epitaxial silicene on Ag(111) by oxygen intercalation. *Sci. Adv.* **2**, e1600067 (2016).

Quasi-freestanding epitaxial silicene on Ag(111) by oxygen intercalation

Yi Du, Jincheng Zhuang, Jiaou Wang, Zhi Li, Hongsheng Liu, Jijun Zhao, Xun Xu, Haifeng Feng, Lan Chen, Kehui Wu, Xiaolin Wang and Shi Xue Dou

Sci Adv **2** (7), e1600067.
DOI: 10.1126/sciadv.1600067